Environmental Science and Pollution Research (2022) 29:25685–25693
https://doi.org/10.1007/s11356-021-17749-z

RESEARCH ARTICLE

Volcanic rock powder residues as precursors for the synthesis of adsorbents and potential application in the removal of dyes and metals from water

Diovani L. Rossatto[1] · Matias S. Netto[1] · Glaydson S. Reis[2] · Luis F. O. Silva[3] · Guilherme L. Dotto[1]

Received: 3 September 2021 / Accepted: 21 November 2021 / Published online: 30 November 2021

Abstract

The present study verified the potential of volcanic rock powder residues originating from the extraction of semi-precious rocks in the state of Rio Grande do Sul, Brazil, as precursors or adsorbents for dyes and metallic ion removal from water. In this way, it is possible to add value and give an adequate destination to this waste. Volcanic rock powder residues from Ametista do Sul (AME) and Nova Prata (NP) were the starting materials. These were used naturally or submitted to the alkaline activation process at 60 °C and alkaline fusion at 550 °C. The analysis of the starting samples by X-ray fluorescence (XRF) revealed that they are mainly composed of aluminum, calcium, iron, and silicon oxides, which corroborates the presence of numerous crystalline phases observed in the X-ray diffraction spectra (XRD). Moreover, by XRD analysis of the synthesized samples, alkaline fusion proved to be more efficient in the dissolution of crystalline phases and consequently in the formation of the amorphous phase (more reactive). Furthermore, the adsorption tests with acid green and acid red dyes and Ag^{+}, Co^{2+}, and Cu^{2+} ions indicated the viability of using residual volcanic rock powder as raw material for the production of adsorbents functionalized with sodium hydroxide, being that the samples synthesized by alkaline fusion showed better results of removal and adsorption capacity for all the contaminants used in the study.

Keywords Adsorbent · Adsorption · Volcanic rock · Alkaline activation · Alkaline fusion

Introduction

The state of Rio Grande do Sul (RS), located in the southern region of Brazil, concentrates a large number of mines for the exploration of semi-precious volcanic rocks (amethyst, agate, etc.) for ornamental purposes (Hartmann et al. 2015; Petrakis et al. 2010). The mining region of Ametista do Sul, for example, stands out as one of the largest producers of amethyst geodes in the world, with average exploration between the years 2016 to 2017 in the order of 380 tons/month; around 95% of the production was exported to Asia, the USA, and Europe, and the rest remained in the domestic market (Dalla Valle and Dorr 2020). Although an important economic activity for the state of RS, it simultaneously generates rock powder waste as an environmental passive, normally stored in the open (Pinto and Hartmann 2011). According to the Cooperative of Energy and Rural Development of Middle Uruguay (COOGAMAI), the accumulation of waste, only for the Ametista do Sul region, is 15,000 tons per month. Another city in RS, recognized for generating large amounts of volcanic rock waste, is Nova Prata, with about 10,000 tons/year according to the Quarry Extraction Industry Syndicate of Rio Grande do Sul.

The industrial residue of volcanic rock waste, most often stored in the open air on mine slopes, can reach and contaminate (due to the concentration of chemical species such as nutrients and metals present) the water bodies through their fragmentation and transport through the rainwater (Ontiveros-Cuadras et al. 2018; Vosoogh et al. 2016). According to Remor et al. (2018) these materials are

Responsible Editor: Philippe Garrigues

✉ Guilherme L. Dotto
guilherme_dotto@yahoo.com.br

[1] Chemical Engineering Department, Federal University of Santa Maria, Santa Maria 97105-900, Brazil

[2] Department of Forest Biomaterials and Technology, Swedish University of Agricultural Sciences, 90183 Umeå, Sweden

[3] Department of Civil and Environmental, Universidad de La Costa, CUC, Calle 58 # 55–66, Barranquilla, Atlántico, Colombia

subject to adsorption, complexation, and precipitation processes when entering the aquatic environment. As a result, they tend to decant, becoming part of the sediments. Thus, sediment contamination by chemical elements, such as metals and nutrients, due to their bioavailability, bioaccumulation, persistence, and possible toxicity constitutes a threat to aquatic ecosystems (Silva et al. 2016; Pejman et al. 2015). Furthermore, Ontiveros-Cuadras et al. (2018) and Vosoogh et al. (2016) reported that, in the mining regions, the concentrations of chemical species being in the sediments of water bodies are higher than that of chemical species background levels and may pose environmental risks. At the moment, the correct management of waste represents one of the most urgent and important issues addressed by science and technology. Thus, there is an increasing search for the efficient use of mined materials to eliminate or mitigate environmental impacts.

Due to the chemical composition of the waste rock powder, studies have sought to verify their potential as an adsorbent, being this applied directly or functionalized with another element (Zhu et al. 2015; Asere et al. 2017; Tejeda et al. 2017; Bugarčić et al. 2018; Chao et al. 2019). Recently, alkaline activated materials, such as geopolymers, have been gaining space in adsorption studies, and very promising results have been achieved in treating effluents containing dyes (Vieira et al. 2021). Chao et al. (2019) synthesized a volcanic rock-based ceramsite adsorbent for selective fluoride removal. The fluoride adsorption capacity was 10.16 mg g^{-1} at 298 K. Bugarčić et al. (2018) sought to determine the potential of raw volcanic rock as an adsorbent of heavy metals in anionic form (chromates, Cr; arsenates, As; and selenates, Se). The equilibrium adsorption capacities for As, Cr, and Se were 12.6, 15.6, and 9.29 mg g^{-1}, respectively. Tejeda et al. (2017) evaluated and compared the adsorption capacity of carbamazepine by the raw volcanic rock (tezontle) and its modification by biofilm growth. The adsorption capacity of raw tezontle was 3.48 µg g^{-1}. On the other hand, for the tezontle with biofilm, the minimum value was 1.75 µg g^{-1} (after the second week of adsorption), and the maximum was 3.3 µg g^{-1} (after 6 months). Ultimately, Choi et al. (2014) activated volcanic rock powder with NaOH and evaluated its adsorption potential for ammonium nitrogen and phosphate and the influence of the alkalinizing agent (NaOH) concentration used in the synthesis.

In front of that and allied to the abundance and regionality of rock powder tailings, this article aims to evaluate the adsorbent potential of volcanic rock powder from the Ametista do Sul and Nova Prata mines, either by direct application or functionalized by alkaline activation for the treatment of water contaminated with acid green 16 (AG16) and acid red 97 (AR 97) dyes and metal ions (Ag^{+}, Co^{2+}, and Cu^{2+}), which represent a serious environmental problem and the health of living beings when eliminated in wastewater, such as cancer, mutation, kidney damage, and toxicology (Malhotra et al. 2020; Rossatto et al. 2020; Gómez et al. 2018; Jeon 2017; Leyssens et al. 2017; Bui et al. 2016). Thus, in addition to the appropriate destination to be given to rock powder tailings and adding value to them, it will be possible to prevent contaminants from polluting the environment when used in wastewater treatment.

Material and methods

Materials, chemicals products, and contaminants

Samples of volcanic rock powder residues come from mining companies in Ametista do Sul and Nova Prata (Rio Grande do Sul, Brazil). Sigma-Aldrich supplied sodium hydroxide PA (NaOH) in microbeads. The dyes acid green 16 (AG 16, molar weight = 560.62 g mol^{-1}, $\lambda_{máx}$ = 640 nm) and acid red 97 (AR 97, molar weight = 698.63 g mol^{-1}, $\lambda_{máx}$ = 498 nm), both with 99% purity, were acquired from Danny Color Corantes (Brazil) and Sigma-Aldrich, respectively, while the silver nitrate ($AgNO_3$, molar weight = 169.87 g mol^{-1}), cobalt (II) chloride ($CoCl_2$, molar weight = 129.84 g mol^{-1}), and copper (II) sulfate ($CuSO_4{\cdot}5H_2O$, molar weight = 249.69 g mol^{-1}), all with PA purity grade, were purchased from INLAB (Brazil). Deionized water (electrical conductivity = 0.9 µS cm^{-1} and electrical resistivity = 1.1 MΩ cm) was used to prepare materials and all solutions.

Synthesis and sample characterization techniques

Initially, the NaOH was manually ground and then mixed with samples of volcanic rock powder from Ametista do Sul (AME) and Nova Prata (NP). Then a sufficient amount of deionized water to form a paste was added, generating in this way two samples with volcanic rock powder from Ametista do Sul and two others with that of Nova Prata. Afterward, the samples were submitted to heat treatment in an oven (alkaline activation) and muffle (alkaline fusion). Table 1 shows the operating conditions for the preparation of materials. Then, the samples were washed with deionized water

Table 1 Operating conditions in the synthesis of new adsorbent materials from volcanic rock powder

Volcanic rock (VR)	Samples	Mass ratio VR/NaOH	Temperature (°C)	Reaction time (min)
Ametista do Sul	AME.A	1	60	360
Ametista do Sul	AME.F	1	550	90
Nova Prata	NP.A	1	60	360
Nova Prata	NP.F	1	550	90

and vacuum filtered until neutral pH, and finally, they were dried in an oven at 100 °C for 8 h, thus obtaining the new materials. These preparation routes were developed after a series of experimental tests performed in our laboratory.

Fourier-transform infrared spectroscopy (FTIR) analysis was used to characterize the samples to evidence the presence of functional groups through the Shimadzu spectrophotometer (IR Prestige 21 model), operating in the wavenumber range from 4,000 to 400 cm^{-1} and sample prepared together with KBr. The resolution and the number of scans of the FTIR spectrum are 2.0 and 45, respectively. In addition, an X-ray fluorescence spectrometer (Rigaku RIX 3000) was used to determine the amount of the main compounds in all samples. The mineralogical composition of the samples was evaluated by the X-ray diffraction (XRD) method using a Rigaku diffractometer, model Miniflex 300, operated with Cu-Kα radiation (λ = 1,5419 Å), 30 kV, 10 mA, scan range 5.0 to 99.98 degrees, step size of 0.03°, and a counting time of 0.5 s per step. The surface properties of the samples, specific surface area, pore-volume, and pore size distribution were determined by the Brunauer–Emmett–Teller (BET) and Barret-Joyner-Halenda (BJH) method. The specific surface area was estimated by applying the BET method at a P/P0 value between 0.06 and 0.3, while the pore volume and pore size distributions were determined by the BJH method. The pore volume was quantified by the volume of nitrogen adsorbed at a P/P0 pressure ratio of 0.98 (Barrett et al. 1951).

Adsorption tests

Batch adsorption experiments were performed to verify contaminants' adsorption capacity and removal percentages from aqueous solutions using precursor materials and alkaline activated from these (AME, AME.A, AME.F, NP, NP.A, NP.F). The operating parameters were stirring speed of 150 rpm, solution volume of 25 mL, and adsorbent dosage of 1 g L^{-1}, initial contaminant concentration of 50 mg L^{-1}, and adsorption time of 2 h. The tests were conducted with digital temperature control (298 K) in a Dubnoff Orbital bath tank (Nova, Brazil). First, the aqueous solutions of the contaminants used for adsorption were prepared from stock solutions (1.00 g L^{-1}) of the dyes AG 16, and AR 97, of Ag^{+} (silver nitrate, $AgNO_3$), Co^{2+} (cobalt(II) chloride, $CoCl_2$), and Cu^{2+} (copper(II) sulfate, $CuSO_4$), and later the experiments were carried out by diluting the stock solution in deionized water. According to preliminary tests, the pH of the aqueous dye solutions was 2.3, while the pH of the metals was that of the solution itself (silver = 6.61, copper = 5.28, and cobalt = 6.59). The experiments were performed in triplicates.

At the end of each adsorption experiment, samples were collected, centrifuged/filtered, and the residual concentration of the contaminant in the solution was determined. For dyes, a Kasuaki UV–VIS spectrophotometer, model IL-226-NM, was used and for metals an Agilent Technologies atomic absorption spectrophotometer, model 240 FS AA. Equation (1) was used to determine the adsorption capacity (q, mg g^{-1}), and Eq. (2) was used to determine the removal percentage (RE, %):

$$q = \frac{(C_0 - C_r)V}{m} \quad (1)$$

$$RE = \frac{(C_0 - C_r)100}{C_0} \quad (2)$$

where C_0 is the initial concentration of the contaminant in the solution (mg L^{-1}), C_r is the residual concentration of the contaminant in the solution (mg L^{-1}), m is the amount of adsorbent (g), and V is the volume of the solution (L).

Results and discussion

Characteristics of volcanic rock powder residues and their derived adsorbents

The main compounds present in the volcanic rock powder samples, AME and NP, obtained by XRF, are described in Table 2. From the analysis of Table 2, it is verified that the precursor samples of rock powder AME and NP have a very similar chemical composition, with variations only in the amount of each compound, which are similar to those reported by Korchagin et al. (2019) and Dalmora et al. (2020), respectively. The silicon and aluminum oxides present in the samples are essential components for synthesizing materials by alkaline activation, such as geopolymers (Zhuang et al. 2016). The presence of alkali oxides (Na_2O and K_2O) in the samples may indicate alkali feldspars

Table 2 Main oxides present in AME and NP volcanic rock powder samples

Oxides	Volcanic rock powder (mass %)	
	AME	NP
SiO_2	47.32	62.10
Al_2O_3	15.60	13.35
Fe_2O_3	14.15	7.96
CaO	8.27	4.26
MgO	4.96	2.88
Na_2O	3.56	3.07
TiO_2	3.27	1.05
K_2O	1.65	3.14
P_2O_5	0.86	0.27
Total	99.64	98.08

(Ndjock et al. 2017). The chemical composition results by XRF confirm that the precursor samples under study come from typical minerals of volcanic rocks (Bugarčić et al. 2018; Korchagin et al. 2019).

The XRD patterns of volcanic rock powders and their synthesized materials (Fig. 1) show a mixture of amorphous and crystalline phases composed of the primary minerals feldspar [albite (PDF: 3323), andesine (AMCSD: 1052), anorthite (PDF: 1257), labradorite (AMCSD: 757), microcline (PDF: 3850), and nephenile (PDF: 3059)], pyroxenes [augite (PDF: 7242), diopside (PDF: 3008), enstatite (PDF: 3407), and pigeonite (AMCSD: 209)], olivines [forsterite (PDF: 0016) and fayalite (PDF: 8155)], opaque minerals [hematite (PDF: 1062), magnetite (PDF: 5151), and maghemite (AMCSD: 7898)], mica [muscovite (PDF: 3548)], and

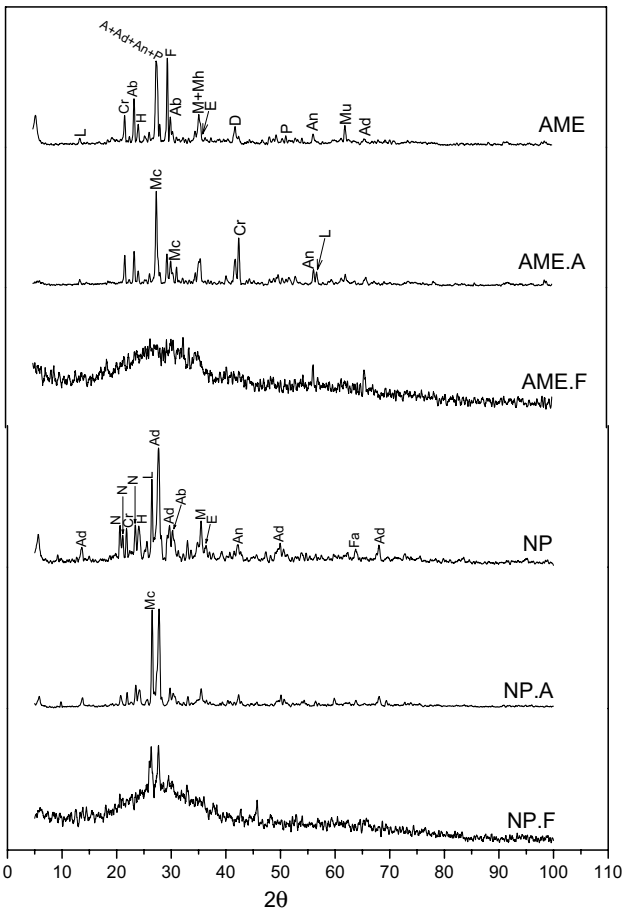

Fig. 1 XRD patterns of volcanic rocks (AME and NP) and materials synthesized by alkaline activation/fusion (AME.A, AME.F, NP.A, and NP.F). A: augite—$(Ca, Mg, Fe)_2Si_2O_6$, Ab: albite—$Na(AlSi_3O_8)$, Ad: andesine—$(Na, Ca)(Si, Al)_4O_8$, An: anorthite—$Ca(Al_2Si_2O_8)$, Cr: cristobalite—SiO_2, D: diopside—$CaMgSi_2O_6$, E: enstatite—$Mg_2Si_2O_6$, F: forsterite—Mg_2SiO_4, Fa: fayalite—Fe_2SiO_4, H: hematite—Fe_2O_3, L: labradorite—$(Ca, Na)(Si, Al)_4O_8$, M: magnetite—Fe_3O_4, Mc: microcline—$K(AlSi_3O_8)$, Mh: maghemite—$\gamma-Fe_2O_3$, Mu: muscovite—$KAl_2(Si_3Al)O_{10}(OH)_2$, N: nepheline—$Na_3K(Al_4Si_4O_{16})$ e P: pigeonite—$(Mg, Fe, Ca)_2Si_2O_6$

cristobalite (PDF: 7924). In the AME.F and NP.F spectra, the transformation of the phases of the starting materials after the alkaline fusion process is clear, observing the presence of an amorphous halo between 18 and 40° (2θ) and practically the absence of crystalline peaks, being evidence of crystalline phase dissolution (Duxson et al. 2007). On the other hand, the existence of starting minerals in the AME.A and NP.A sample indicates the opposite: the absence or incomplete dissolution of the crystalline phases observed in the pure volcanic rock samples (Lemougna et al. 2014). According to Duxson et al. (2007), the precipitation and dissolution of an aluminosilicate depend on several factors, such as temperature, Si/Al ratio, and pH, so it can be suggested that the difference found between the diffractograms of the synthesized materials ".A" and ".F" is the synthesis temperature. The appearance of the microcline (Mc) crystalline phase in the AME.A and NP.A spectra, and labradorite in AME.A, is also due to the alkaline activation in the starting volcanic rocks (Çetintaş and Soyer-Uzun 2018).

Figure 2 shows the FTIR spectra of volcanic rock powder samples and materials synthesized by alkaline activation. The wide bands 3434 to 3445 cm^{-1} present in all materials are behaviors attributed to bending and O–H elongation of the silanols and the remaining adsorbed water (Giannopoulou and Panias 2010; Yankwa Djobo et al. 2016a, b). The absorption bands in the region of 1635 to 1647 cm^{-1} represent the H–O–H bending vibrations of the bound water molecules, which can be absorbed by the surface or trapped in the material structure after adsorption of atmospheric water due to the cooling of volcanic magma (Tchakoute Kouamo et al. 2012). In the NP.F sample, the weak band at 1472 cm^{-1} is due to O–C–O elongation vibrations related to the vibrational modes of carbonates, which suggests the occurrence of atmospheric carbonation after alkaline fusion (Sarkar

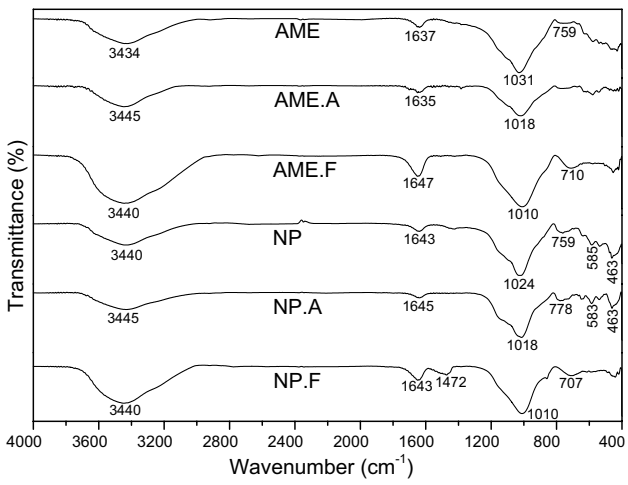

Fig. 2 FTIR spectra of starting volcanic rocks and synthesized materials

et al. 2018; Giannopoulou and Panias 2010). In the IR spectra of the precursor samples (AME and NP), the 1024 and 1031 cm^{-1} vibration bands are designated by the Si–O–T asymmetric elongation (T: Al or Si) (Yankwa Djobo et al. 2016b). According to Tchadjié et al. (2016), these bands are typical of the presence of the mineral albite, which corroborates the results obtained in XRD. After the alkaline activation process, they changed to 1010 and 1018 cm^{-1}, indicating the amorphous aluminosilicate gel phase (Tchakoute et al. 2013). According to Yunsheng et al. (2010), this change to smaller wavenumbers can be referred to as the partial replacement of the tetrahedron of SiO_4 by the AlO_4 due to the change in the local chemical environment of the bond Si–O. The bands in the range 778 to 707 cm^{-1} are related to bending vibrations –Si–O–Si– in molecules $(SiO_2)_n$. There are differences between the different silica compounds in this range, such as quartz and cristobalite (Sitarz et al. 2000). The appearance of these bands in the AME.F (710 cm^{-1}) and NP.F (707 cm^{-1}) samples, in lower wavenumbers compared to their precursors (759 cm^{-1}), can be attributed to the formation of amorphous to semi-crystalline aluminosilicate (Panias et al. 2007) and which is in agreement with what is shown in the XRD data. The 463 cm^{-1} band is characteristic of the silicate mesh's Si–O elongation vibrations (Yankwa Djobo et al. 2016a).

The physical characteristics of the materials studied in this article are shown in Table 3. It is verified that all the synthesized materials have a specific surface area and total pore volume greater than their precursor. The higher their values, the better the adsorption capacity of the material can be (Hosseinzadeh et al. 2015). Besides, the materials produced by alkaline fusion (AME.F and NP.F) presented expressive increases in the specific surface area and total pore volume than the materials obtained by activation (AME.A and NP.A). These results can be explained based on the synthesis procedures and follow FTIR and XRD. AME.F and NP.F were produced at 550 °C, leading to its precursors' efficient crystalline phase dissolution. Otherwise, AME.A and NP.A were produced at 60 °C, leading to a partial dissolution of the crystalline phase.

The adsorption and desorption isotherms of N_2 and the pore size distributions of the precursor and synthesized materials are shown in Fig. 3a and b, respectively. The isotherms (Fig. 3a) reveal that they are classified, according to the IUPAC, as type IV and hysteresis loop H3 format, indicating mesopores' existence (Thommes 2010). Moreover, the presence in all samples of the vertical asymptotic profile for high values of P/P_0 suggests that the structures are meso- and macroporous with non-uniform size and slit-shaped pores. The analysis of Fig. 3b shows the predominance of mesopores (2 nm ≤ pore diameter ≤ 50 nm) in all samples, corroborating with the predicted by the N_2 adsorption–desorption isotherms and a small incidence of macropores.

Table 3 Physical characteristics of the studied samples

Sample	Specific surface area ($m^2\ g^{-1}$)	Average pore diameter (nm)	Total pore volume ($cm^3\ g^{-1}$)
AME	8.17	11.34	0.023
AME.A	14.66	7.24	0.026
AME.F	129.82	6.66	0.216
NP	14.99	15.18	0.032
NP.A	16.62	10.86	0.045
NP.F	39.99	11.76	0.118

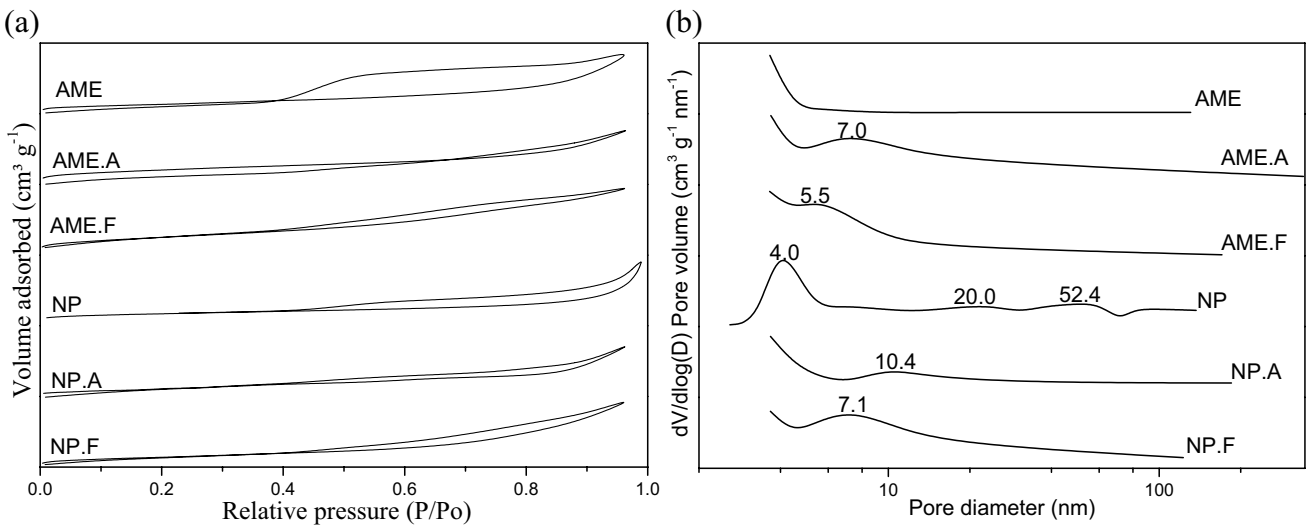

Fig. 3 **a** N_2 adsorption–desorption isotherms and **b** pore size distribution of precursor samples and synthesized materials

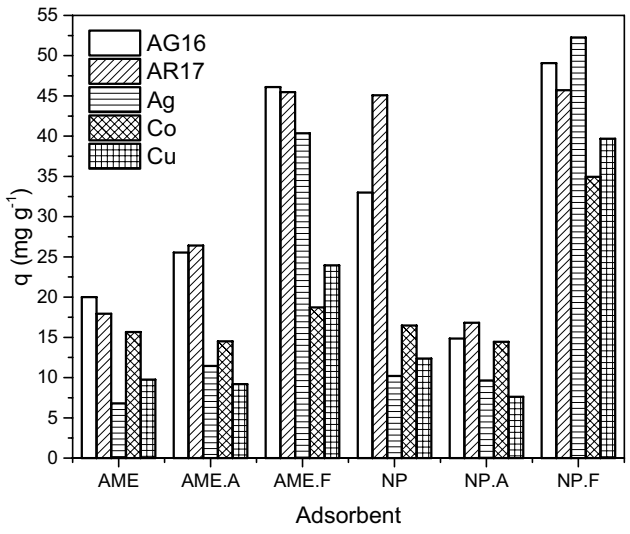

Fig. 4 Results of adsorption capacity (q) for dye acid green 16 (AG 16) and acid red 97 (AR 97) and metal ion silver (Ag), cobalt (Co), and copper (Cu), performed with the starting and synthesized samples

The adsorptive potential of volcanic rock powder residues and their derived adsorbents

The adsorption tests of dyes and metals, performed with the starting and synthesized samples (AME, AME.A, AME.F, NP, NP.A, NP.F), are shown in Fig. 4. It was verified that the samples produced by alkaline fusion AME.F and NP.F obtained better results than their precursors (AME and NP) for all contaminants. For example, the adsorption and removal capacity of the acid green 16 dye was 49 mg g^{-1} and 97.6% for NP.F, respectively, while its precursor (NP) was 32 mg g^{-1} and 67%, respectively. Besides, AME.F and NP.F presented better adsorption performance than the samples synthesized by alkaline activation (AME.A and NP.A) for all used contaminants. However, between these two, the NP.F sample proved to be more efficient, reaching removal capabilities (RE) and adsorption (q) greater than 90% and 40 mg g^{-1}, respectively, except for cobalt where $RE = 63.15\%$ and $q = 34.95$ mg g^{-1}. This trend can be explained based on the characteristics of the material. Based on Fig. 1, greater amorphization of the starting samples was found in the alkaline fusion process. This behavior makes the material more reactive than its precursor. Furthermore, as shown in Table 3, AME.F presented a surface area 16 times higher than AME and 9 times higher than AME.A. A similar profile was verified for the pore-volume values. In parallel, NP.F presented a surface area around 2.5 times higher than NP and NP.A (Table 3).

Table 4 compares the sorption capacity of various adsorbents used in adsorption of different acid red and acid green dyes and metallic ions silver, cobalt, and copper. This table shows that the NP.F synthesized sample presented greater or very close to the greater adsorption capacity of the evaluated contaminants. Although not shown, the same can be observed for the AME.F sample for the adsorption of dyes and Ag ions. Therefore, it can be suggested that both samples have a great potential to be adsorbents of the studied contaminants. The NP.F sample is the most prospective

Table 4 Comparison of the adsorption capacity of several adsorbents used in the adsorption of the contaminants studied in this article

Adsorbent	Adsorbate	pH	T (K)	q (mg g^{-1})	References
Low-moor peat and smectite	AG dye	5.67	298	13.10	Kyziol-Komosinska et al. (2015)
Activated *Prunus Dulcis*		2	323	50.79	Jain and Gogate (2018)
Magnetic chitosan nanocomposite		5.4	298	26.2	Mohamad and Prasad (2014)
NP.F		2.3	298	49.07	This work
Citrus limonum peels	AR dye	2	303	0.62	Latif et al. (2018)
Activated carbon from fibrous		2	298	21.68	Salman Naeem et al. (2018)
Activated carbon		-	298	55.25	Gómez et al. (2007)
NP.F		2.3	298	45.71	This work
Colloidal carbon nanospheres	Ag^{+}	-	298	152.00	Song et al. (2011)
Verde-lodo bentonite		4–5	293	9.72	Freitas et al. (2017)
Waste coffee grounds		6	298	46.20	Jeon (2017)
NP.F		6.83	298	52.26	This work
Verde-lodo bentonite	Cu^{2+}	4–5	333	6.99	Freitas et al. (2017)
Pretreated Maize Husk		5.5	298	35.71	Duru et al. (2019)
NP.F		5.78	298	39.69	This work
Organosilicas	Co^{2+}	8	298	37.31	Lee et al. (2016)
Alginate nanoparticles		6.5	298	33.56	El-Shamy et al. (2019)
Mesoporous carbon		6	298	4.10	Gómez et al. (2018)
NP.F		6.60	298	34.96	This work

choice among all tested materials since it possesses the highest adsorption capacity toward various pollutants.

Conclusion

Samples of volcanic rock powder from the cities of Ametista do Sul (AME) and Nova Prata (NP), both residues abundant in the Rio Grande do Sul, Brazil, showed a low adsorption capacity and removal efficiency of the dyes acid red 97 and acid green 16, as well as for the metallic ions of Ag^{+}, Co^{2+}, and Cu^{2+}. However, this ability was improved from the functionalization of precursor samples through alkaline activation/fusion with sodium hydroxide (NaOH). The samples synthesized by alkaline fusion, AME.F, and NP.F were the ones that achieved the best results, since, according to the XRD results, it was the process capable of dissolving with greater efficiency the crystalline phases of the starting samples, thus making the materials amorphous and more reactive. These results suggest the potential of volcanic rock powder residues, studied here, as raw material in the synthesis of adsorbents for acid green 16 and acid red 97 dyes and metallic ions and maybe even for other contaminants present in effluents and water, being a suitable alternative for the disposal of tons of volcanic rock powder residues which accumulate in the semi-precious stone geode extraction mines in the Rio Grande do Sul.

Author contribution Conceptualization: D. L. Rossatto, G. L. Dotto, and L. F. O. Silva. Methodology: D. L. Rossatto and M. S. Netto. Formal analysis and investigation: D. L. Rossatto and M. S. Netto. Writing—original draft preparation: D. L. Rossatto, G. L. Dotto, and M. S. Netto. Writing—review and editing: D. L. Rossatto, G. S. Reis, and M. S. Netto. Funding acquisition: G. L. Dotto and L. F. O. Silva. Supervision: L. F. O. Silva and G. L. Dotto. All authors read and approved the final manuscript.

Funding The authors would like to thank CAPES (Coordination for the Improvement of Higher Education Personnel) and CNPq (National Council for Scientific and Technological Development) for their financial support.

Availability of data and materials The datasets used and/or analyzed during the current study are available from the corresponding author on reasonable request.

Declarations

Ethical approval Not applicable.

Consent to participate Not applicable.

Consent to publish Not applicable.

Competing Interests The authors declare no competing interests.

References

Asere TG, Verbeken K, Tessema DA, Fufa F, Stevens CV, Du Laing G (2017) Adsorption of As(III) versus As(V) from aqueous solutions by cerium-loaded volcanic rocks. Environ Sci Pollut Res 24:20446–20458. https://doi.org/10.1007/s11356-017-9692-z

Barrett EP, Joyner LG, Halenda PP (1951) The determination of pore volume and area distributions in porous substances. I. Computations from Nitrogen Isotherms. J Amer Chem Soc 73:373–380. https://doi.org/10.1021/ja01145a126

Bugarčić MD, Milivojević M, Marinković A, Marković B, Sokić M, Petronijević N, Stojanović J (2018) Application of raw volcanic rock found in Etna valley as an adsorbent of chromates, arsenates and selenates. Metall Mater Eng 24:133–144. https://doi.org/10.30544/366

Bui TKL, Do-Hong LC, Dao TS, Hoang TC (2016) Copper toxicity and the influence of water quality of Dongnai River and Mekong River waters on copper bioavailability and toxicity to three tropical species. Chemosphere 144:872–878. https://doi.org/10.1016/j.chemosphere.2015.09.058

Çetintaş R, Soyer-Uzun S (2018) Relations between structural characteristics and compressive strength in volcanic ash based one–part geopolymer systems. J Build Eng 20:130–136. https://doi.org/10.1016/j.jobe.2018.07.011

Chao C, Zhao Y, Song Q, Min J, Wang Z, Ma H, Li X (2019) Volcanic rock-based ceramsite adsorbent for highly selective fluoride removal: function optimization and mechanism. J Chem Technol Biotechnol 94:2263–2273. https://doi.org/10.1002/jctb.6014

Choi JW, Ryu JC, Kwon KS, Song MK, Lee S, Kim SB, Lee SH (2014) Adsorption of ammonium nitrogen and phosphate onto basanite and evaluation of toxicity. Water Air Soil Pollut 225:2059. https://doi.org/10.1007/s11270-014-2059-x

Dalla Valle C, Dorr AC (2020) A Comercialização de Pedras Preciosas No Mercado Nacional e Internacional: Uma Análise Da Região Do Médio Alto Uruguai Do Rio Grande Do Sul. Revista Científica Hermes (in Portuguese) 27:252–273

Dalmora AC, Ramos CG, Plata LG, da Costa ML, Kautzmann RM, Oliveira LFS (2020) Understanding the mobility of potential nutrients in rock mining by-products: an opportunity for more sustainable agriculture and mining. Sci Total Environ 710:136240. https://doi.org/10.1016/j.scitotenv.2019.136240

Duru CE, Duru IA, Ogbonna CE, Enedoh MC, Emele P (2019) Adsorption of copper ions from aqueous solution onto natural and pretreated maize husk: adsorption efficiency and kinetic studies. J Chem Soc Nigeria 44:798–803

Duxson P, Fernández-JiménezA PJL, Lukey GC, Palomo A, Van Deventer JSJ (2007) Geopolymer technology: the current state of the art. J Mater Sci 42:2917–2933. https://doi.org/10.1007/s10853-006-0637-z

El-Shamy OAA, El-Azabawy RE, El-Azabawy OE (2019) Synthesis and characterization of magnetite-alginate nanoparticles for enhancement of nickel and cobalt ion adsorption from wastewater. J Nanomater 2019:6326012. https://doi.org/10.1155/2019/6326012

Freitas ED, Carmo ACR, Almeida Neto AF, Vieira MGA (2017) Binary adsorption of silver and copper on Verde-lodo bentonite: kinetic and equilibrium study. Appl Clay Sci 137:69–76. https://doi.org/10.1016/j.clay.2016.12.016

Giannopoulou I, Panias D (2010) Hydrolytic stability of sodium silicate gels in the presence of aluminum. J Mater Sci 45:5370–5377. https://doi.org/10.1007/s10853-010-4586-1

Gómez V, Larrechi MS, Callao MP (2007) Kinetic and adsorption study of acid dye removal using activated carbon. Chemosphere 69:1151–1158. https://doi.org/10.1016/j.chemosphere.2007.03.076

Gómez JM, Díez E, Bernabé I, Sáez P, Rodríguez A (2018) Effective adsorptive removal of cobalt using mesoporous carbons synthesized by silica gel replica method. Environ Process 5:225–242. https://doi.org/10.1007/s40710-018-0304-9

Hartmann LA, Medeiros JTN, Baggio SB, Antunes LM (2015) Controls on prolate and oblate geode geometries in the Veia Alta basalt flow, largest world producer of amethyst, Paraná volcanic province, Brazil. Ore Geol Ver 66:243–251. https://doi.org/10.1016/j.oregeorev.2014.11.005

Hosseinzadeh H, Zoroufi S, Mahdavinia GR (2015) Study on adsorption of cationic dye on novel kappa-carrageenan/poly(vinyl alcohol)/montmorillonite nanocomposite hydrogels. Polym Bull 72:339–1363. https://doi.org/10.1007/s00289-015-1340-5

Jain SN, Gogate PR (2018) Efficient removal of Acid Green 25 dye from wastewater using activated Prunus Dulcis as biosorbent: batch and column studies. J Environ Manage 210:226–238. https://doi.org/10.1016/j.jenvman.2018.01.008

Jeon C (2017) Adsorption of silver ions from industrial wastewater using waste coffee grounds. Korean J Chem Eng 34:384–391. https://doi.org/10.1007/s11814-016-0253-9

Korchagin J, Caner L, Bortoluzzi EC (2019) Variability of amethyst mining waste: a mineralogical and geochemical approach to evaluate the potential use in agriculture. J Clean Prod 210:749–758. https://doi.org/10.1016/j.jclepro.2018.11.039

Kyziol-Komosinska J, Rosik-Dulewska C, Pajak M, Czupiol J, Dzieniszewska A, Krzyzewska I (2015) Sorption of Acid Green 16 from aqueous solution onto low-moor peat and smectite clay co-occurring in lignite of Belchatow mine field. Annu Set Environ Prot 17:165–187

Latif S, Rehman R, Imran M, Iqbal S (2018) Biosorptive decontamination of acid red-87 dye from wastewater by citrus limonum peels: ecofriendly approach. Pakistan J Anal Environ Chem 19:44–52. https://doi.org/10.21743/pjaec/2018.06.04

Lee SH, Park SS, Parambadath S, Ha CS (2016) Sulphonic acid functionalized periodic mesoporous organosilica with the bridged bissilylated urea groups for high selective adsorption of cobalt ion from artificial seawater. Micro Meso Mater 226:179–190. https://doi.org/10.1016/j.micromeso.2015.10.047

Lemougna PN, Chinje Melo UF, Delplancke MP, Rahier H (2014) Influence of the chemical and mineralogical composition on the reactivity of volcanic ashes during alkali activation. Ceram Int 40:811–820. https://doi.org/10.1016/j.ceramint.2013.06.072

Leyssens L, Vinck B, Van Der Straeten C, Wuyts F, Maes L (2017) Cobalt toxicity in humans - a review of the potential sources and systemic health effects. Toxicol 387:43–56. https://doi.org/10.1016/j.tox.2017.05.015

Malhotra N, Ger TR, Uapipatanakul B, Huang JC, Chen KHC, Hsiao CD (2020) Review of copper and copper nanoparticle toxicity in fish. Nanomater 10:1–28. https://doi.org/10.3390/nano10061126

Mohamad M, Prasad B (2014) Chemical design of smart chitosan/polypyrrole/magnetite nanocomposite toward efficient water treatment. Phys Chem Chem Phys 16:21812–21819. https://doi.org/10.1039/C4CP03062A

Ndjock BDL, Elimbi A, Cyr M (2017) Rational utilization of volcanic ashes based on factors affecting their alkaline activation. J Non Cryst Solids 463:31–39. https://doi.org/10.1016/j.jnoncrysol.2017.02.024

Ontiveros-Cuadras JF, Ruiz-Fernández AC, Sanchez-Cabeza JA, Pérez-Bernal LH, Preda M, Páez-Osuna F (2018) Mineralogical signatures and sources of recent sediment in a large tropical lake. Int J Sediment Res 33:183–190. https://doi.org/10.1016/j.ijsrc.2017.12.002

Panias D, Giannopoulou IP, Perraki T (2007) Effect of synthesis parameters on the mechanical properties of fly ash-based geopolymers. Colloids Surf A Physicochem Eng Asp 301:246–254. https://doi.org/10.1016/j.colsurfa.2006.12.064

Pejman A, Bidhendi GN, Ardestani M, Saeedi M, Baghvand A (2015) A new index for assessing heavy metals contamination in sediments: a case study. Ecol Ind 58:365–373. https://doi.org/10.1016/j.ecolind.2015.06.012

Petrakis GH, Motoki A, Sichel SE, Zucco LL, Aires JR, Mello SLM (2010) Geologia de jazidas de brita e areia artificial de qualidade especial: Exemplos do álcali sienito de Nova Iguaçu, RJ, e riolito de Nova Prata, RS (In portuguese). Geociencias 29:21–32

Pinto VM, Hartmann LA (2011) Flow-by-flow chemical stratigraphy and evolution of thirteen Serra Geral Group basalt flows from Vista Alegre, southernmost Brazil. An Acad Braz Cienc 83:425–440. https://doi.org/10.1590/S0001-37652011000200006

Remor MB, Sampaio SC, Rijk S, Vilas Boas MA, Gotardo JT, Pinto ET, Schardong FA (2018) Sediment geochemistry of the urban Lake Paulo Gorski. Int J Sediment Res 33:406–414. https://doi.org/10.1016/j.ijsrc.2018.04.009

Rossatto DL, Netto MS, Jahn SL, Mallmann ES, Dotto GL, Foletto EL (2020) Highly efficient adsorption performance of a novel magnetic geopolymer/Fe3O4 composite towards removal of aqueous acid green 16 dye. J Environ Chem Eng 8:103804. https://doi.org/10.1016/j.jece.2020.103804

Salman Naeem M, Javed S, Baheti V, Wiener J, Javed MU, Ul Hassan SZ, Mazari A, Naeem J (2018) Adsorption kinetics of acid red on activated carbon web prepared from acrylic fibrous waste. Fibers Polym 19:71–81. https://doi.org/10.1007/s12221-018-7189-5

Sarkar C, Basu JK, Samanta AN (2018) Synthesis of mesoporous geopolymeric powder from LD slag as superior adsorbent for zinc (II) removal. Adv Powder Technol 29:1142–1152. https://doi.org/10.1016/j.apt.2018.02.005

Silva PRB, Makara CN, Munaro AP, Schintlzer DC, Wastowski AD, Poleto C (2016) Comparison of the analytical performance of EDXRF and FAAS techniques in the determination of metal species concentrations using protocol 3050B (USEPA). Int J River Basin Manage 14:401–406. https://doi.org/10.1080/15715124.2016.1203792

Sitarz M, Handke M, Mozgawa W (2000) Identification of silicooxygen rings in SiO2 based on IR spectra. Spectrochim Acta - Part A Mol Biomol Spectrosc 56:1819–1823. https://doi.org/10.1016/S1386-1425(00)00241-9

Song X, Gunawan P, Jiang R, Leong SSJ, Wang K, Xu R (2011) Surface activated carbon nanospheres for fast adsorption of silver ions from aqueous solutions. J Hazard Mater 194:162–168. https://doi.org/10.1016/j.jhazmat.2011.07.076

Tchadjié LN, Djobo JNY, Ranjbar N, Tchakouté HK, Kenne BBD, Elimbi A, Njopwouo D (2016) Potential of using granite waste as raw material for geopolymer synthesis. Ceram Int 42:3046–3055. https://doi.org/10.1016/j.ceramint.2015.10.091

Tchakoute HK, Elimbi A, Yanne E, Djangang CN (2013) Utilization of volcanic ashes for the production of geopolymers cured at ambient temperature. Cem Concr Compos 38:75–81. https://doi.org/10.1016/j.cemconcomp.2013.03.010

Tchakoute Kouamo H, Elimbi A, Mbey JA, Ngally Sabouang CJ, Njopwouo D (2012) The effect of adding alumina-oxide to metakaolin and volcanic ash on geopolymer products: a comparative study. Constr Build Mater 35:960–969. https://doi.org/10.1016/j.conbuildmat.2012.04.023

Adsorption capacity of a volcanic rock-used in constructed wetlands-for carbamazepine removal, and its modification with biofilm growth. Water (Switzerland) 9.https://doi.org/10.3390/w9090721

Thommes M (2010) Physical adsorption characterization of nanoporous materials. Chemie Ing Tech 82:1059–1073. https://doi.org/10.1002/cite.201000064

Vieira Y, Netto MS, Lima EC, Anastopoulos I, Oliveira MLS, Dotto GL (2021) An overview of geological originated materials as a trend for adsorption in wastewater treatment. Geosci Front In press 101150.https://doi.org/10.1016/j.gsf.2021.101150

Vosoogh A, Mohsen S, Raziyeh L (2016) Heavy metals relationship with water and size-fractionated sediments in rivers using canonical correlation analysis (CCA) case study, rivers of south western Caspian Sea. Environ Monit Assess 188:603. https://doi.org/10.1007/s10661-016-5611-x

Yankwa Djobo JN, Elimbi A, Dika Manga J, Ndjock IBDL (2016a) Partial replacement of volcanic ash by bauxite and calcined oyster shell in the synthesis of volcanic ash-based geopolymers. Constr Build Mater 113:673–681. https://doi.org/10.1016/j.conbuildmat.2016.03.104

Yankwa Djobo JN, Elimbi A, Tchakouté HK, Kumar S (2016b) Mechanical activation of volcanic ash for geopolymer synthesis: Effect on reaction kinetics, gel characteristics, physical and mechanical properties. RSC Adv 6:39106–39117. https://doi.org/10.1039/c6ra03667h

Yunsheng Z, Wei S, Zongjin L (2010) Composition design and microstructural characterization of calcined kaolin-based geopolymer cement. Appl Clay Sci 47:271–275. https://doi.org/10.1016/j.clay.2009.11.002

Zhu X, Song T, Lv Z, Ji G (2015) Removal of Cu(II) and Ni(II) ions from an aqueous solution using α-Fe2O3 nanoparticle-coated volcanic rocks. Water Sci Technol 72:2154–2165. https://doi.org/10.2166/wst.2015.434

Zhuang XY, Chen L, Komarneni S, Zhou CH, Tong DS, Yang HM, Yu WH, Wang H (2016) Fly ash-based geopolymer: clean production, properties and applications. J Clean Prod 125:253–267. https://doi.org/10.1016/j.jclepro.2016.03.019